Computational Geosciences
https://doi.org/10.1007/s10596-024-10286-x

ORIGINAL PAPER

Robust inversion of 1D magnetotelluric data using the Huber loss function

Elfitra Desifatma[1] · I. Gede Putu Fadjar Soerya Djaja[1] · Prihandhanu Mukti Pratomo[1] · Supriyadi[1] · Enjang Jaenal Mustopa[1] · Maria Evita[1] · Mitra Djamal[1] · Wahyu Srigutomo[1]

Received: 21 June 2023 / Accepted: 1 April 2024

Abstract
In this study, a robust 1D inversion was performed on magnetotelluric (MT) data by utilizing the Huber loss function to avoid misleading interpretation of results, which is caused by the presence of outliers in the data. The MT method utilizes the ratio between the electric field (E) and the magnetic field (H), which are perpendicular to each other, to obtain impedance values (Z). These values are used to extract subsurface information in the form of electrical resistivity variations with depth. In the study, forward modeling of the 1D MT responses was conducted by recursively calculating Z values. Robust inversion was performed using the Huber loss function as an objective function to minimize the difference between the calculated and observed data. The Huber loss function combines the squared loss and the absolute loss to anticipate the presence of outliers in MT observation data. The robust inversion was performed on synthetic data with additional noise and field data. The inversion process utilized 50 layers with a thickness of 500 m, a hyperparameter $\delta = 5 \times 10^{-2}$, $\lambda = 0.01$, and $\lambda_t = 100$. The number of iterations used was 500 for inversions that used synthetic data and 3000 for inversions that used field data. The robust inversion scheme using the Huber loss function successfully overcame the presence of outliers and accurately estimated the actual model parameters, both for synthetic data and field data that contained outliers. The misfit was relatively small and close to zero, indicating that the inversion code works well.

Keywords Huber loss · Inverse modeling · Magnetotelluric · Robust inversion · One dimension

1 Introduction

The magnetotelluric (MT) method is a geophysical technique that provides information on the distribution of subsurface electrical conductivity by measuring natural electric $\left(\vec{E}\right)$ and magnetic $\left(\vec{H}\right)$ fields on the surface that vary with time [1–3]. The MT method finds applications in various geophysical investigations, including geothermal [4–8], hydrocarbon [9–12], and mineral investigations [13–15]. It is well-suited for exploring a wide range of depths, from shallow to profound, without the need for artificial sources and without causing environmental damage [16], making it a suitable choice for exploration purposes. Natural MT fields originate from solar storms for low-frequency electromagnetic (EM) fields (< 1 Hz) and lightning activity near the Earth's surface for high frequencies (≥ 1 Hz) [17]. These EM waves propagate towards the Earth's surface, where some are reflected, while others are transmitted into the subsurface. Receivers record the resulting superposition of primary and secondary EM fields. The ratio between the electric field $\left(\vec{E}\right)$ and the magnetic field $\left(\vec{H}\right)$ is expressed as impedance $\vec{Z}$, which is then used to determine the electrical resistivity ρ (Ωm) in the MT modeling.

The MT method is essential in geophysical exploration, so it is widely used to examine the electrical properties of the Earth's subsurface. The presence of outliers in the MT data results in an inappropriate model [18], leading to inaccurate characterization of subsurface structure [19] and misleading interpretations. The outlier removal process can increase the reliability and accuracy of the analysis in data interpretation. Three outlier removal methods are used most often: the impedance estimation by correlation [20–22], the robust method [23–25], and the time serial analysis method [26, 27]. The robust method is widely utilized in terrestrial EM studies,

✉ Wahyu Srigutomo
srigutomo@itb.ac.id

[1] Institut Teknologi Bandung, Jl. Ganesha no 10, Bandung, Jawa Barat, Indonesia

Published online: 23 April 2024

specifically for time series EM data [25, 28–30]. Besides this method's application in MT data processing, several authors have also employed a robust inversion approach, which aims to estimate the subsurface properties of geophysical data by minimizing the impact of outliers or data errors. Inversion refers to the process of transforming measured geophysical data into a subsurface model. Robust inversion techniques are designed to handle situations where the data contain outliers or errors, which can significantly affect the accuracy of the inversion results. In this study, robust inversion was performed using Huber's loss function, which offers protection against outliers in heavy-tailed symmetric distributions [31]. While MT data processing in 2D and 3D domains has seen significant advancements [32–34], one-dimensional (1D) MT data processing still holds significance in assessing data quality [35] and determining the initial model for subsequent 2D and 3D inversions [36]. Generally, MT inversions encounter ill-posed problems [37] and solution stability issues. Regularization is typically employed to address the ill-posed problems of MT inversions by incorporating a stabilization function into the objective function to obtain a stable inversion solution [38]. Moreover, the presence of outlier data often obscures the primary information in MT field data, leading to inaccurate resistivity imaging. Several researchers have conducted MT 1D inversions [39–41] but have not effectively mitigated the presence of outliers. Geophysical inversion problems are commonly addressed using the least-squares (LS) scheme with damping or smoothness constraints to enhance inversion stability and accelerate convergence [42]. However, the conventional LS-based inversion method is sensitive to outliers in electric and magnetic field data, which can result in inappropriate resistivity values [43]. Therefore, a robust inversion algorithm is necessary to overcome or eliminate the presence of outliers in MT field data [43]. In this study, the Huber loss (HB) function was employed as the objective function to achieve robust inversion and mitigate the impact of outliers.

This study aims to develop an effective 1D MT inversion algorithm that reduces the presence of outliers by utilizing the HB function. The HB function combines the useful characteristics of square loss and absolute loss into one loss function to get the best results. This combination is expected to be highly effective in detecting and handling outliers in the data. With the addition of the HB function, the inversion process becomes robust, allowing for the minimization of the impact of outliers.

2 Method

2.1 Forward modeling of 1D magnetotelluric

Impedance can be used to obtain physical information, i.e., apparent resistivity (ρ_{app}) and phase impedance (ϕ). EM impedance [Z] can be written as Eq. 1 [44]:

$$Z = \frac{\omega\mu_0}{\sqrt{-i\mu_0\omega\sigma}} = \sqrt{i}\sqrt{\mu_0\omega\rho} = \sqrt{\mu_0\omega\rho}e^{i\pi/4}, \tag{1}$$

where $k = \sqrt{-i\mu_0\omega\sigma}$; μ_0 is magnetic permeability in vacuum; $\omega = 2\pi f$, with f being frequency; and σ is the conductivity of the medium, which is the inverse of the resistivity $\rho = 1/\sigma$.

Based on Eq. 1, the apparent resistivity equation (ρ_{app}) and phase impedance (ϕ) for anisotropic homogeneous earth can be formulated as:

$$\rho_{app} = \frac{1}{\mu_0\omega}|Z|^2 \tag{2}$$

$$\phi = arctan\left[\frac{Im(Z)}{Re(Z)}\right] \tag{3}$$

For a homogeneous earth, the phase impedance value is $\phi = \frac{\pi}{4}rad = 45^{\circ}$. In real conditions, Earth's subsurface structure in 1D can be illustrated as a layered earth (Fig. 1) that consists of n layers with a thickness of h_n and a resistivity of ρ_n. For a layered earth, the impedance value for the earth model with n layers can be generated based on the following recursive equation:

$$\hat{Z}_n = Z_n\frac{\hat{Z}_{n+1} + \hat{Z}_n\tanh(ik_nh_n)}{\hat{Z}_n + \hat{Z}_{n+1}\tanh(ik_nh_n)} \tag{4}$$

$\hat{Z}_n$ is the impedance in the n^{th} layer due to resistivity variations. Equation 4 is used recursively to get the measured impedance value on the surface, iteratively calculated from the n^{th} layer. For a homogeneous earth model, the

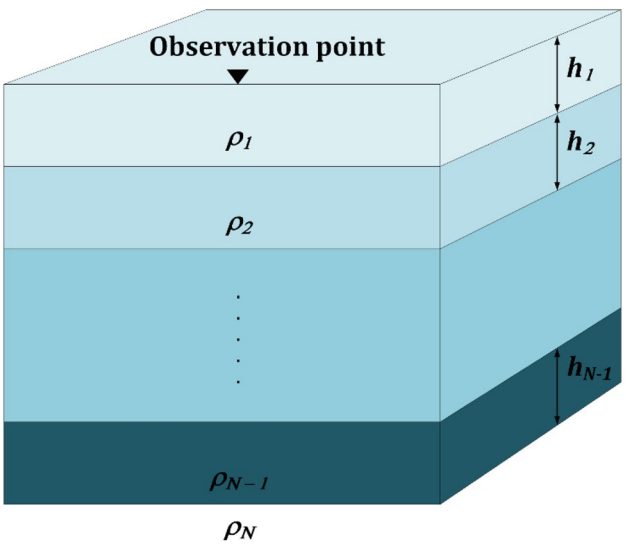

Fig. 1 1D Layered earth illustration

thickness of layer one is set to infinity ($h_1 = \infty$) so that $\tanh(ik_1h_1) = 1$, and the surface impedance becomes

$$\hat{Z}_1 = Z_1$$

or

$$\hat{Z}_N = Z_N,$$

with $Z_n = \frac{\omega\mu_0}{k_n}$ and $k_n = \frac{\sqrt{-i\mu_0\omega}}{\rho_n}$

Forward modeling using a recursive equation (Eq. 4) produces systematic data, which is then used iteratively in the inversion process/scheme. The validation process for the 1D MT forward modeling program was conducted by comparing the response of the modeling results in the form of apparent resistivity to the response from the homogeneous earth model. The apparent resistivity value of the forward modeling results must have the same value as the resistivity value of the homogeneous model, and the phase impedance value of the modeling results must be 45°, which is the phase impedance in the homogeneous model.

2.2 Robust inversion using the Huber loss function

Inversion is a mathematical method for generating information on a physical system in the form of a phenomenon that is reviewed based on observations of the system [45]. Inversion can also be defined as a procedure for estimating physical parameters from observational data [4]. The physical parameters to observe are the model parameters that produce calculated data that matches the observational data. The matching level between the calculated data and the observed data is expressed through the objective function. The objective function is minimized to obtain the final model parameters. Robust inversion aims to remove noise from MT data. This study used robust inversion by utilizing HB as the objective function. The equation for the objective function used can be written as follows:

$$\begin{aligned}\mathbf{L} = &\,\| \Delta\mathbf{d_1} \|_H + \| \Delta\mathbf{d_2} \|_H + \lambda_1 \| \partial(\boldsymbol{m_0} + \Delta\mathbf{m}) \|^2 \\ &+ \lambda_2 \| \mathbf{I}(\Delta\mathbf{m}) \|^2\end{aligned} \tag{5}$$

$$\boldsymbol{L_H}(x_i) = \begin{cases} \| \mathbf{x} \|_H = \sum L_H(x_i) \\ \frac{1}{2}x_i^2 \quad \text{for} |x_i| \le \delta \\ \delta\left(|x_i| - \frac{1}{2}\delta\right) \quad \text{otherwise} \end{cases}, \tag{6}$$

where $\| \mathbf{x} \|_H$ is a misfit in Eq. 5, detailed further in Eq. 6, and $\Delta\mathbf{d}_1 = \mathbf{d}_1 - \mathbf{f}_1(\mathbf{m})$ and $\Delta\mathbf{d}_2 = \mathbf{d}_2 - \mathbf{f}_2(\mathbf{m})$ are the differences between observation and calculation data. The variable $\Delta\mathbf{m} = \mathbf{m} - \mathbf{m_0}$, where $\mathbf{m}$ is the model parameter vector, and $\mathbf{m_0}$ is the initial model parameter. The second and third terms on the right side of Eq. 5 are implementation constraints on the model; the second term is implemented to obtain a smooth model, while the third term is implemented so that the change in $\Delta\boldsymbol{m}$ is not too large. The variables λ_1 and λ_2 are Lagrange multipliers, ∂ is the differential operator, $\boldsymbol{\delta}$ is a hyperparameter, and $\mathbf{I}$ is the identity matrix. The solution to Eq. 5 can be written as follows:

$$\begin{aligned}\mathbf{\Delta m^{k+1}} = &\left(\mathbf{J_1^T W^k J_1} + \mathbf{J_2^T W^k J_2} + \lambda_1\partial^T\partial + \lambda_2\mathbf{I}\right)^{-1} \\ &\left(\mathbf{J_1^T W^k \Delta d_1} + \mathbf{J_2^T W^k \Delta d}_2 - \lambda_1\partial^{\mathbf{T}}\partial\mathbf{m_0}\right)\end{aligned} \tag{7}$$

$$W_{i,i}^{\boldsymbol{k}} = \begin{cases} 1 & \text{for} \left|\Delta d_i - \left(\mathbf{J\Delta m^k}\right)_\mathbf{i}\right| \le \delta \\ \frac{\delta}{\left|\Delta d_i - \left(\mathbf{J\Delta m^k}\right)_\mathbf{i}\right|} & \text{otherwise} \end{cases}, \tag{8}$$

where W is the weight and $W_{i,i}^0 = 1$ in the first iteration and a diagonal matrix in Eq. 8, with J being Jacobian. Model parameters can be obtained by

$$\mathbf{m} = \mathbf{m_0} + \mathbf{\Delta m^K} \tag{9}$$

Meanwhile, the Jacobian matrix J can be written as follows:

$$\mathbf{J}_1 = \begin{bmatrix} \frac{\partial log_{10}(d_{a1})}{\partial log_{10}\rho_1} & \cdots & \frac{\partial log_{10}(d_{a1})}{\partial log_{10}\rho_N} \\ \vdots & \ddots & \vdots \\ \frac{\partial log_{10}(d_{aM})}{\partial log_{10}\rho_1} & \cdots & \frac{\partial log_{10}(d_{aM})}{\partial log_{10}\rho_N} \end{bmatrix} \tag{10}$$

and

$$\mathbf{J}_2 = \begin{bmatrix} \frac{\partial log_{10}(d_{b1})}{\partial log_{10}\rho_1} & \cdots & \frac{\partial log_{10}(d_{b1})}{\partial log_{10}\rho_N} \\ \vdots & \ddots & \vdots \\ \frac{\partial log_{10}(d_{bM})}{\partial log_{10}\rho_1} & \cdots & \frac{\partial log_{10}(d_{bM})}{\partial log_{10}\rho_N} \end{bmatrix}, \tag{11}$$

where data 1:

$$\begin{aligned} d_{cal1} &= d_a = log_{10}\left(Re(Z)^2 + Im(Z)^2\right) \\ \frac{\partial log_{10}(d_{cal1})}{\partial log_{10}\rho_n} &= 2\left[Re(Z)Re\frac{\partial Z}{\partial \rho_n} + Im(Z)Im\frac{\partial Z}{\partial \rho_n}\right]\frac{\rho_n}{(Re(Z))^2+(Im(Z))^2} \end{aligned} \tag{12}$$

and data 2:

$$\begin{aligned} d_{cal2} &= d_b = log_{10}\frac{(Re(Z))^2}{(Im(Z))^2} \\ \frac{\partial log_{10}(d_{cal2})}{\partial log_{10}\rho_n} &= 2\rho_n\left[\frac{1}{Im(Zz)}Im\frac{\partial Z}{\partial \rho_n} - \frac{1}{Re(Zz)}Re\frac{\partial Z}{\partial \rho_n}\right] \end{aligned} \tag{13}$$

The inversion process is conducted iteratively and will stop if the iteration has reached a maximum or the misfit ($\| d_{obs} - d_{cal} \|^H$) has not changed much from the previous iteration.

3 Result

3.1 Syntetic models

In our study, forward modeling was performed to generate synthetic data in the form of apparent resistivity and phase impedance. This was achieved by applying a synthetic model with predetermined resistivity values and thickness. The synthetic data were utilized to validate the developed inversion code. Three-layer earth models were employed in the forward modeling process to observe the resulting patterns of apparent resistivity and phase impedance. The parameters of the three-layer model used are provided in Table 1.

Before the inversion scheme, the forward modeling of 1D MT using the recursive technique was validated using a homogeneous earth model with a resistivity of 100 Ωm. The results of this forward modeling are depicted in Fig. 2. The apparent resistivity values returned to their homogeneous resistivity value of 100 Ωm, and the phase impedance was consistently 45° for each frequency. Therefore, it could be concluded that the forward modeling code was valid. The homogeneous model was used to test the performance of the forward modeling scheme because, analytically, the forward modeling for a homogeneous earth model is frequency independent (where the apparent resistivity is the same as the true resistivity).

Synthetic data were employed to validate the generated inversion code. The calculated data results from the inversion process had to align with the synthetic (observed) data obtained through forward modeling. The inversion results needed to show high accuracy, whereas the inversion model had to be the same as the test model. For the inversion process, two models with parameters, as presented in Table 1, were utilized to generate synthetic data. Model 1 represented a 3-layer earth model with a conductive layer between the resistive layers, while Model 2 represented a 3-layer earth model with a resistive layer between the conductive layers. Model 1 was used because it referred to several real conditions in the field. An example of this condition is a water-saturated layer in a hydrothermal water environment

Table 1 Synthetic Model Parameters Used to Generate Synthetic Data

Model	Resistivity, ρ (Ωm)			Thickness, h (m)		
	Layer 1	Layer 2	Layer 3	Layer 1	Layer 2	Layer 3
1	100	10	100	500	500	∞
2	10	100	10	500	500	∞

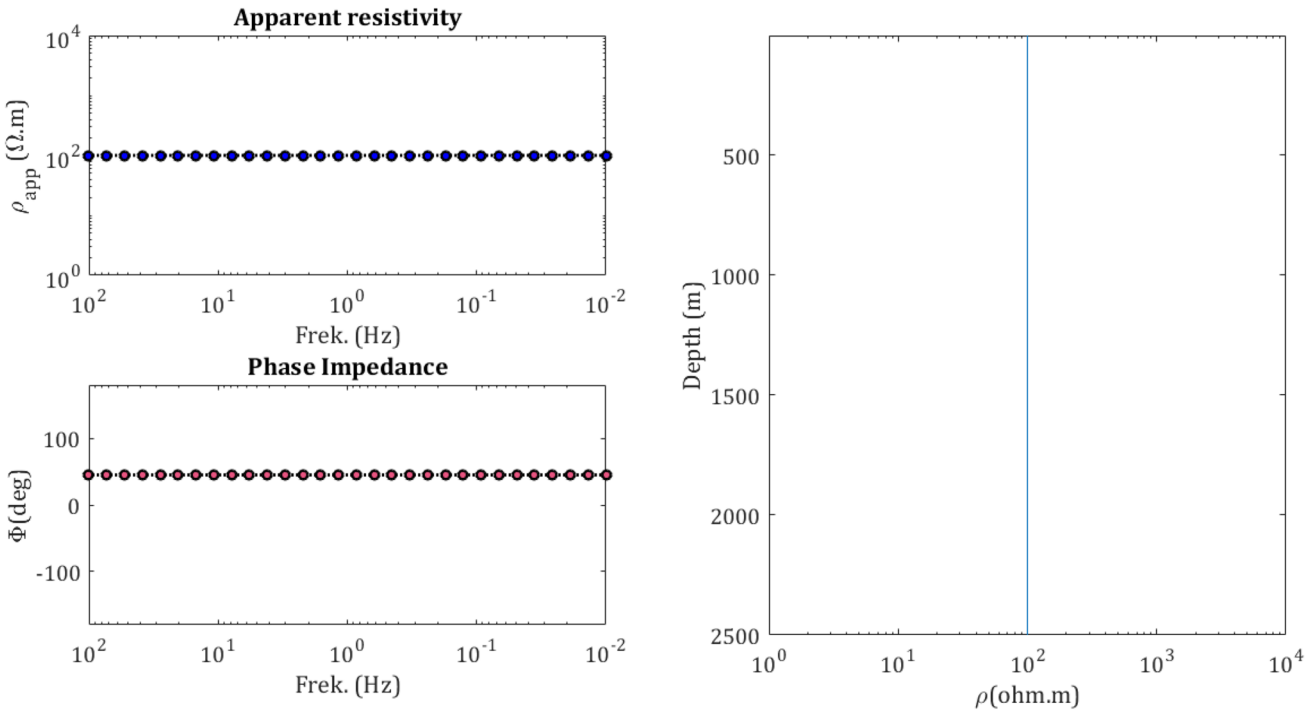

Fig. 2 Response for the homogeneous earth model

filled with hot water from geothermal sources due to fault activity and magma intrusion, which can result in cracks in the basement [46]. Model 2 was also used to refer to real field conditions. An example is a highly resistive granite basement covered with a layer of conductive sediment [47]. During a TDEM survey in the Unzen Mountains of Japan, three main layers were identified: a resistive surface layer, a conductive layer, and a third resistive layer [48]. Outliers were introduced to the synthetic data to simulate real-world scenarios where field data often contain outliers. The chosen inversion scheme was robust inversion using HB, with the LS inversion as a comparison.

The inversion results for Model 1 are presented in Fig. 3. The inversion results demonstrate a close fit between the calculated data and the synthetic data for both the HB and LS inversion schemes. No significant discrepancy was observed between the HB and LS inversion results. The inversion results reveal conductive anomalies between the resistive layers at depths ranging from 200 m to 2000 m. For the HB inversion, convergence was achieved at the 168th iteration out of 500, with a misfit of 0.00009964. The LS inversion reached convergence at the 180th iteration out of 500, with a misfit of 0.00009970. A comparison of the calculated data, synthetic data, and the weight values (W_1 and W_2) for Model 1 is depicted in Fig. 3d and e. The calculation data resulting from the inversion (d_a and d_b) exhibited strong agreement with the synthetic data for both HB and LS inversions. The weight

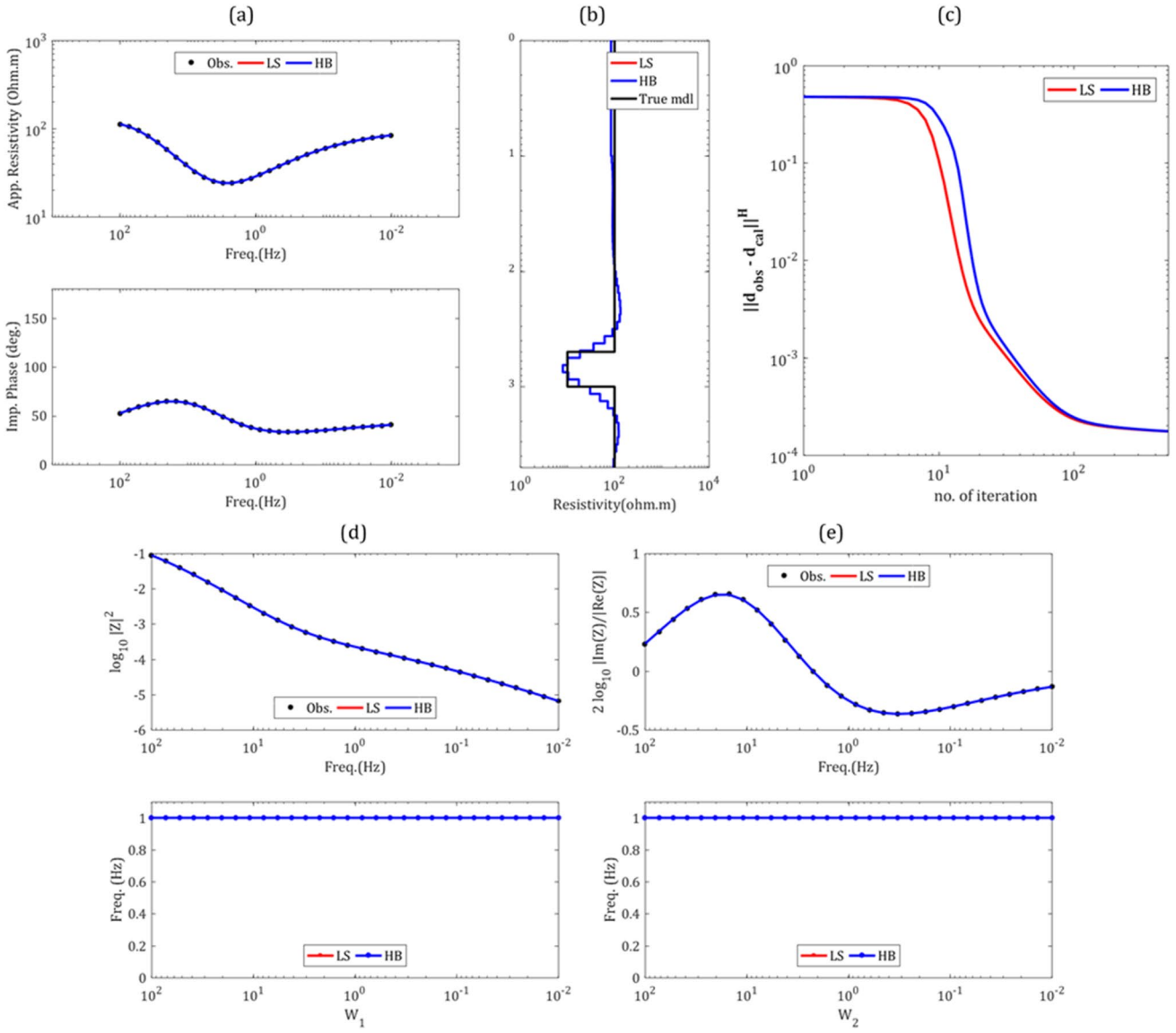

Fig. 3 Huber loss (HB) vs. least-squares (LS) inversion model results Model 1 **a** The inversion result, **b** The inversion result of the model, **c** Misfit, **d** Results of the inversion of data 1 and weight, **e** Results of the inversion of data 2 and weight

values (W_1 and W_2) were both 1 at each frequency since no outliers were present in the data.

The inversion results for Model 2 are displayed in Fig. 4. Similar to those obtained from Model 1 inversion, the calculated data aligned closely with the synthetic data for both the HB and LS inversion approaches. For the HB inversion, convergence was achieved at the 141st iteration out of 500, yielding a misfit of 0.000205. The LS inversion reached convergence at the 154th iteration out of 500, resulting in a misfit of 0.000205. A comparison between the calculated and synthetic data and the corresponding weights is shown in Fig. 4a and e. Similar to Model 1, the inversion process for Model 2 yielded consistent outcomes. The calculated data (d_a and d_b) from the inversion exhibited compatibility with the synthetic data for both HB and LS inversions. The weight values (W_1 and W_2) remained constant at 1 for all frequencies.

Based on the inversion results obtained for both synthetic models, the misfit was significantly small and was approaching zero, indicating the effectiveness of the HB and LS inversion codes. The weights assigned to each frequency were identical due to the absence of outliers in the data, resulting in similar inversion outcomes for both the HB and LS methods. When the inversion results for the two models presented in Figs. 3 and 4 were compared, it became evident that the 1D MT inversion can handle conductive structures (Model 1) more effectively than resistive structures (Model 2). The MT method exhibited greater sensitivity in detecting

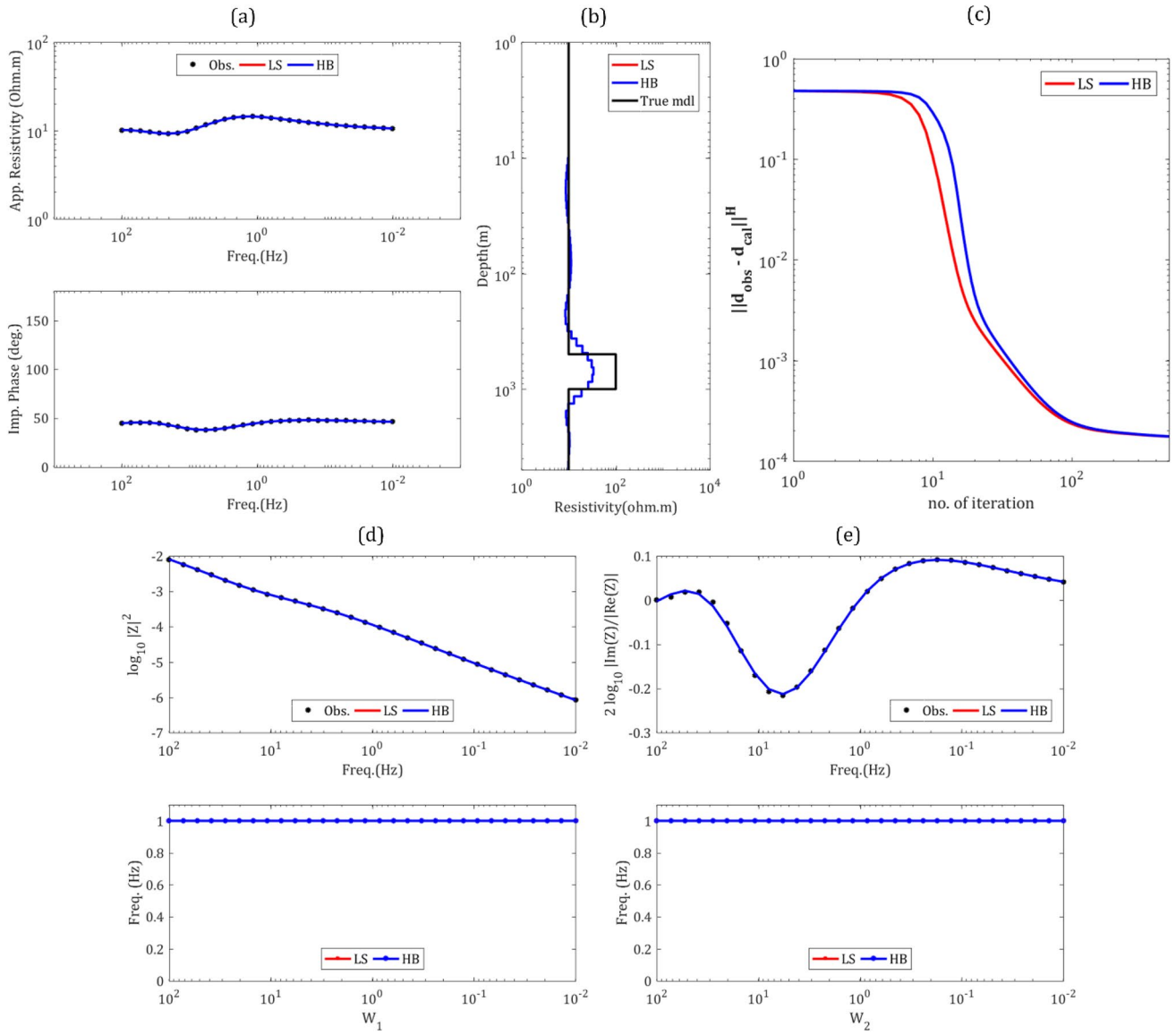

Fig. 4 Huber loss (HB) vs. least-squares (LS) inversion model results Model 2 **a** The inversion result, **b** The inversion result of the model, **c** Misfit, **d** Results of the inversion of data 1 and weight, **e** Results of the inversion of data 2 and weight

conductive structures than resistive structures. According to [49], MT is a sensitive method for detecting low resistivity (high conductivity) structures, which can be caused by various mechanisms such as partial melting, sulfides, metallic minerals, and nominally anhydrous hydrogen.

To gain further insights into the performance of HB and LS inversions, particularly their applicability to field data, outlier data were added to synthetic data from Model 1. The results of the HB and LS inversions for Model 1 with the addition of outliers to their synthetic data, resembling field data, are depicted in Fig. 5. The HB inversion results demonstrate that the calculated data still aligned well with the synthetic data, even in the presence of outliers. Conversely, the LS inversion results show that the calculated data conformed to the synthetic data in the section without outliers but failed to match the calculated data in the section containing outliers (Fig. 5a). In terms of the inversion model, the HB inversion exhibited a strong agreement with the actual model, while the LS inversion displayed some deviations beyond a depth of 1000 m (Fig. 5b). The HB inversion attained convergence at the 25th iteration out of 500, yielding a misfit of 0.1937 (Fig. 5c). On the other hand, the LS inversion reached convergence at the 58th iteration out of 500, resulting in a misfit of 0.2350 (Fig. 5c). The HB inversion assigned appropriate weights to d_a and d_b, where data points identified as outliers within the HB framework were

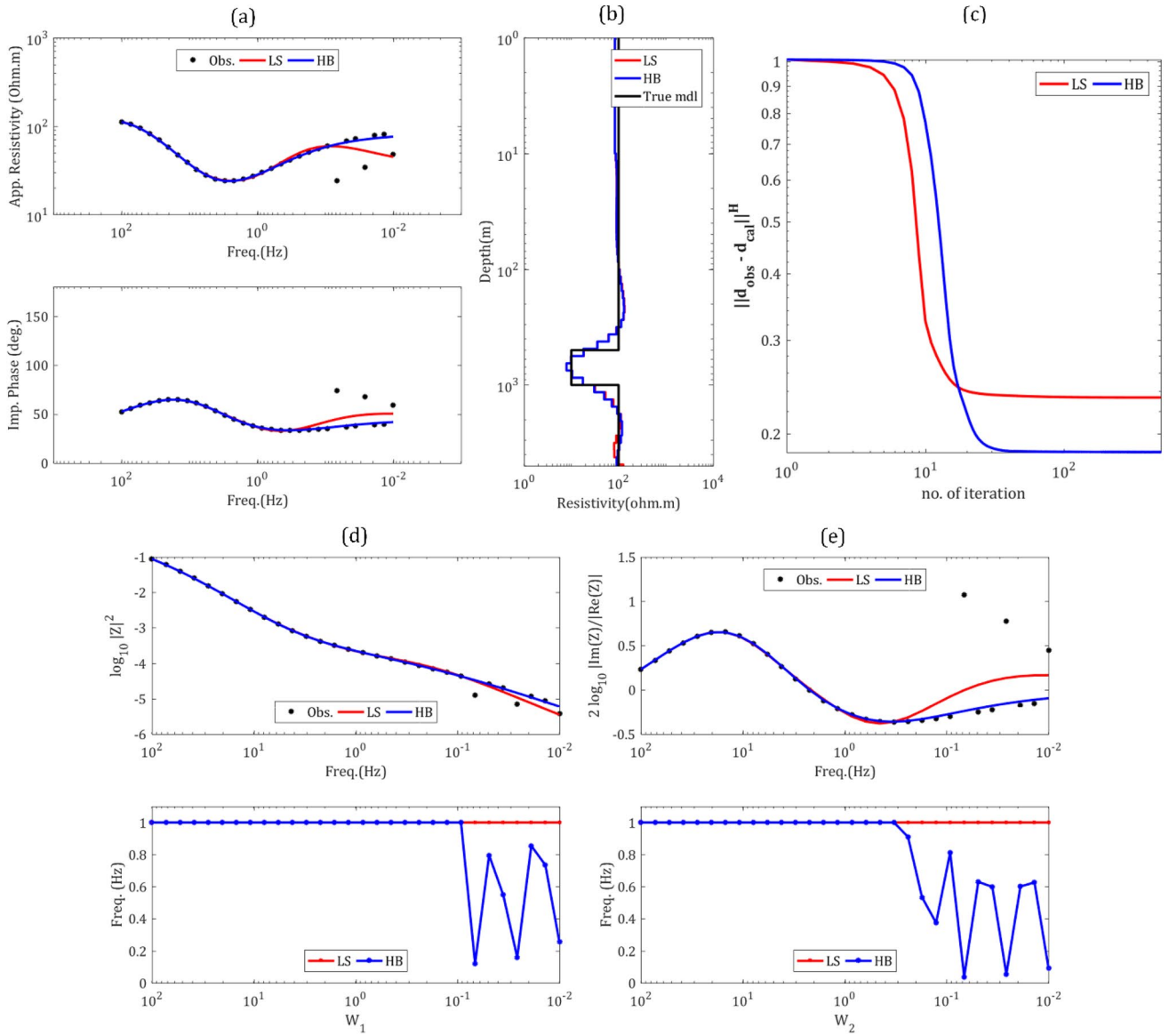

Fig. 5 Huber loss (HB) vs. least-squares (LS) inversion model results with outlier data were added to Model 1 **a** The inversion result in the Model 1 response, **b** The inversion result of the model, **c** Misfit, **d** Results of the inversion of data 1 and weight, **e** Results of the inversion of data 2 and weight

assigned lower weights, as depicted in Fig. 5d and e. When the results of the two inversions in Model 1 with the inclusion of outlier data were compared, it became evident that the HB inversion outperforms the LS inversion in handling data containing outliers. Hence, the HB inversion can be regarded as a robust inversion technique capable of handling the presence of outlier data in field applications. Both inversions were applied to the same field data in Indonesia to provide further verification.

3.2 Application to field data

The inversion was further tested on field data using two inversion schemes. Four sets of data from different locations were employed for this inversion (Fig. 6). Data were collected from four islands in Indonesia, namely MT data in the Patuha area, MT data in the Matindok area, MT data in the Muara Laboh area, and MT data in the Ulumbu area. The location of each measurement area can be seen in Fig. 6. Data for the Patuha area, point MTP-xy, and data for the Matindok area, point MTM-yx, were classified as good-quality data. On the other hand, data for the Muara Laboh area point MTML-xy and data for the Ulumbu area point MTU-xy were classified as poor-quality data. Good-quality data were characterized by smooth data with small errors or deviations and reasonable values within the range of resistivity values for geological materials based on Table 2. Poor-quality data had the opposite characteristics: the data were not smooth, the error or deviation was large with many outliers, and the values did not make sense.

For both inversion schemes, 50 layers were utilized, along with hyperparameters $\delta = 5 \times 10^{-2}$, $\lambda = 0.01$, and $\lambda_t = 100$. The inversion process involved 3000 iterations.

The MT data-xy inversion results for the Patuha area are shown in Fig. 7. The data for the Patuha area at the MTP-xy point (frequency range 318 Hz–0.000992 Hz) exhibited very good quality with no outliers. These data were included in the good-quality data category based on the data criteria mentioned previously. There were no outliers in the data, the data were smooth, the errors or deviations were small, and the values were reasonable. No significant difference was found in the results between the HB and LS inversions. The inversion model revealed the presence of conductive

Table 2 Rock resistivity value [50]

Material	Resistivity (Ωm)
Air	~
Pyrite	0.01–100
Quartz	500–800,000
Calcite	1×10^{12}–1×10^{13}
Rock salt	30–1×10^{13}
Granite	200–10,000
Andesite	170–450,000
Wet	1000–40,000
Dry	10–1.3×10^{7}
Limestone	500–10,000
Sandstone	200–8000
Shales	20–2000
Sand	1–1000
Clay	1–100
Ground water	0.5–300
Sea water	0.2
Magnetite	0.01–1000
Dry gravel	600–10,000
Alluvium	10–800

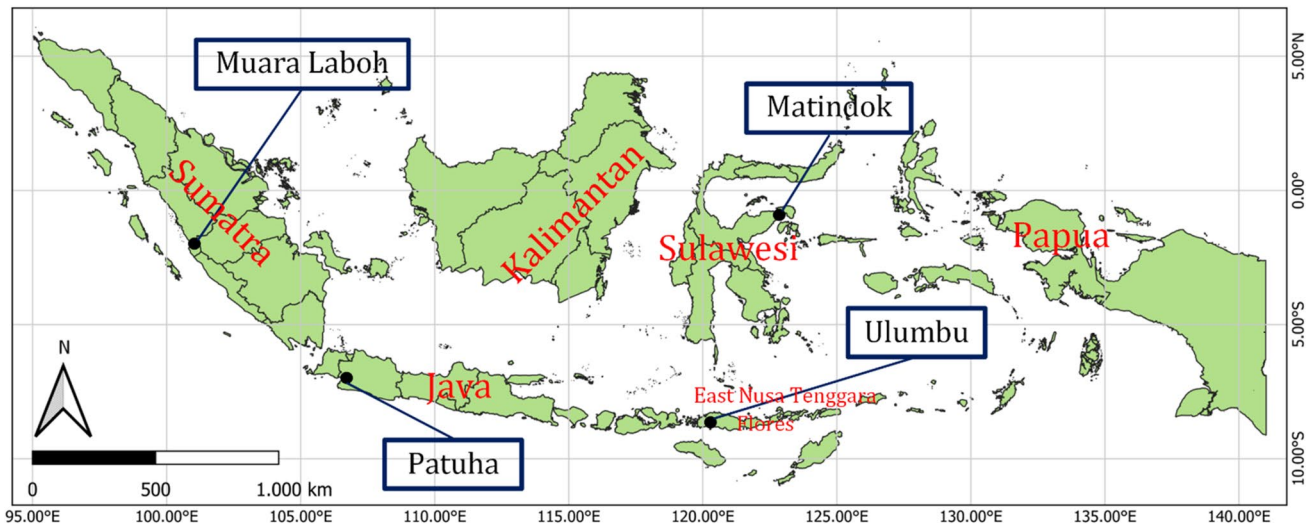

Fig. 6 Map of data measurement points

anomalies between resistive layers at a depth of 200 m to 350 m (Fig. 7b). The HB inversion reached convergence at the 37th iteration out of 1000 iterations, with a misfit of 0.06953 (Fig. 7c). The LS inversion reached convergence at the 20th iteration out of 1000 iterations, with a misfit of 0.07038 (Fig. 7c). A comparison between the observed data and calculated data, along with the weight values for each data d_a andd_b, are shown in Fig. 7d and e. The calculated inversion data for d_a matched the observed data for both HB and LS inversions.

The weight value (W_1) for most HB inversions was one, except in the low-frequency range (10^{-3}–10^{-4} Hz). Similarly, the calculated data for the inversion results for d_b also matched the observed data for both HB and LS inversions. The weight value (W_2) for most HB inversions was one, except in the low-frequency range (10^{-3}–0.000992 Hz).

The results of the data-yx inversion for the Matindok area are shown in Fig. 8. The data for the Matindok area at the MTM-yx point (frequency range 320 Hz–0.00114 Hz) were of good quality, with only a few outliers in the low-frequency section. MT data were still considered good-quality data based on the previously mentioned criteria. In the data, No outliers were found in the data, the error or deviation was small, the data were smooth, and the values were reasonable. There were minor differences in the results between the HB and LS inversion. The inversion model revealed the

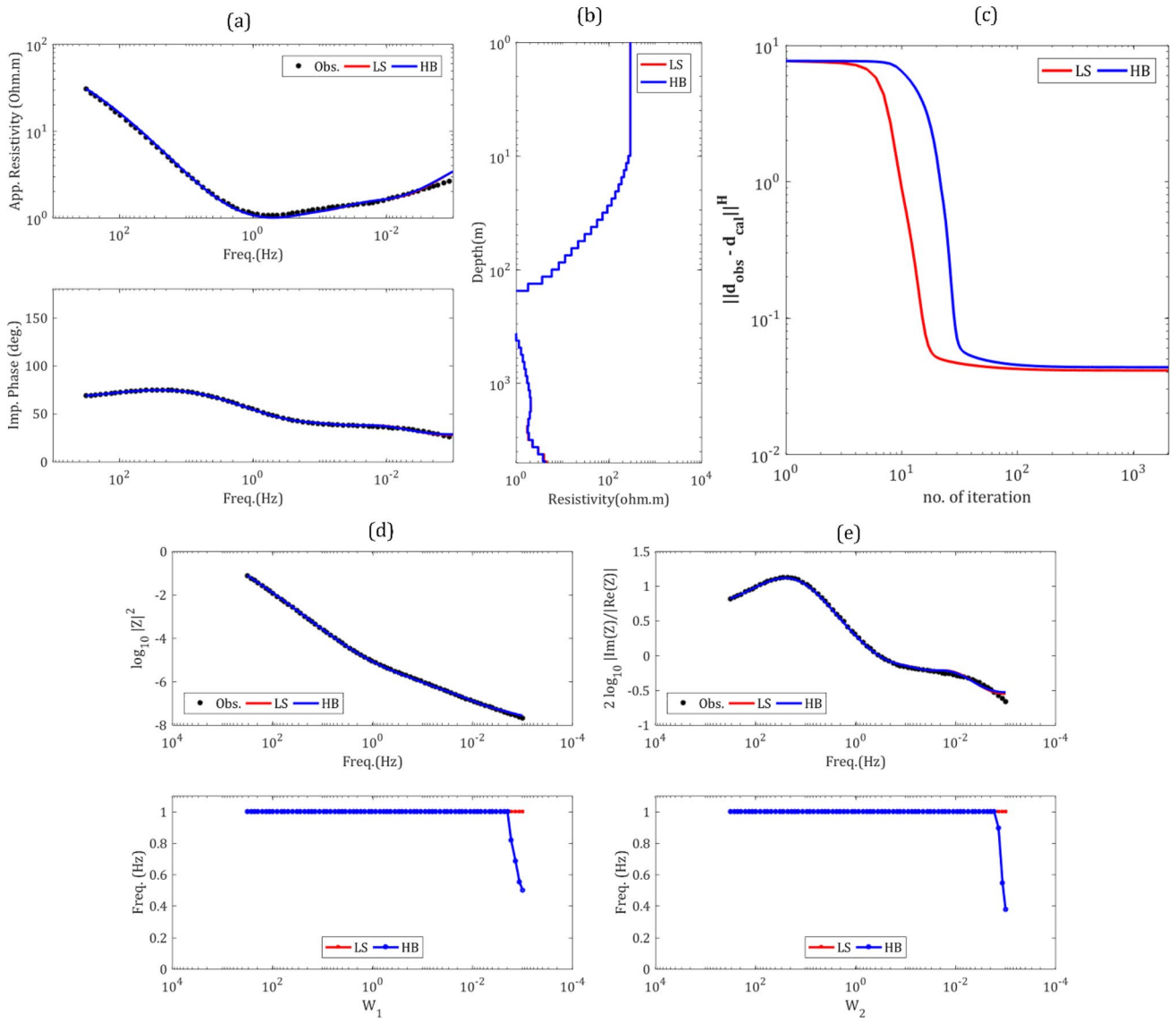

Fig. 7 Huber loss (HB) vs. least-squares (LS) inversion model results for the Patuha MTP-xy area **a** Inversion results of the model response, **b** The inversion result of the model, **c** Misfit, **d** Results of the inversion of data 1 and weights, and **e** Results of the inversion of data 2 and weights

presence of conductive and resistive anomalies that varied at depths ranging from 10 m to 1000 m (Fig. 8b). The HB inversion reached convergence at the 60th iteration out of 3,000 iterations, with a misfit of 0.3069 (Fig. 8c). The LS inversion, on the other hand, initially reached a minimum misfit at the 75th iteration out of 3,000 iterations; however, the misfit gradually increased to 0.3326 at the maximum iteration (Fig. 8c). Comparisons between the observed data and calculated data, as well as the weight values for each data d_a and d_b, are shown in Fig. 8d and e. The calculated inversion data for d_a matched the observed data for both HB and LS inversions. The weight value (W_1) for most HB inversions was one, except in the low-frequency range (1 Hz–0.00114 Hz). Similarly, the calculated inversion data for d_b also matched the observed data for both HB and LS inversions. The weight value (W_2) for the HB inversion exhibited the same pattern as d_a.

The results of the data-xy inversion for the Muara Laboh area can be seen in Fig. 9. The data for the Muara Laboh area at the MTML-xy point (frequency range 10,000 Hz–0.0178 Hz) were of poor quality, based on the previously mentioned criteria. The MT Muara Laboh data contained an unreasonable resistivity value. Normally, geothermal areas tend to have resistivity values that continue to rise at low frequencies, and there are conductive zones that transition into the resistive zone due to a water-saturated layer filled with hot water. However, in the frequency data of 0.1 Hz and below, a decrease in

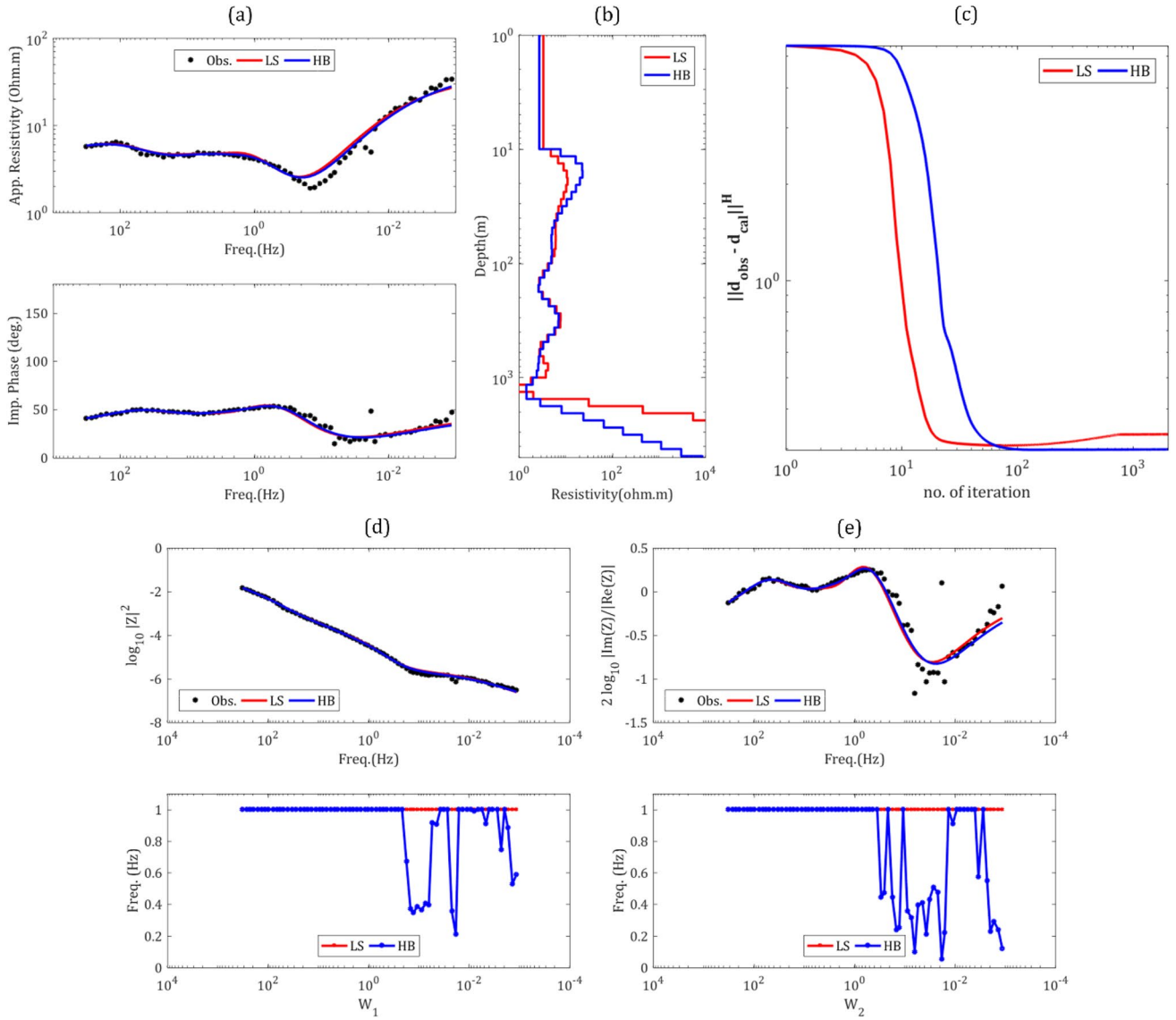

Fig. 8 Huber loss (HB) vs. least-squares (LS) inversion model results for Matindok MTM-yx area (**a**) Inversion results of model response, (**b**) The inversion result model, (**c**) Misfit, (**d**) Results of the inversion of data 1 and weights, (**e**) Results of the inversion of data 2 and weights

resistivity was observed. Differences were observed in the results between the HB and LS inversions, particularly at small frequencies (3 Hz–0.01 Hz), where the LS inversion results deviated slightly from the observed data (Fig. 9a). The results of the HB inversion model showed the presence of conductive anomalies at depths ranging from 100 m to 1000 m and resistive anomalies at depths ranging from 1000 m to 10,000 m. Similar anomalies were also observed in the LS inversion. However, with a larger deviation at depths ranging from 1000 m to 10,000 m, they exhibited resistivity values exceeding 10,000 m (Fig. 9b). The HB inversion reached convergence at the 152nd iteration out of 3000 iterations, with a misfit of 0.1848. On the other hand, the LS inversion initially achieved a minimum misfit at the 44th iteration out of 3000 iterations; however, the misfit gradually increased to 0.3137 at the maximum iteration (Fig. 9c). The comparison between the observed data and the calculated data, as well as the weight values for each data d_a and d_b, are shown in Fig. 9d and e. The calculated inversion data for d_a demonstrated a good fit with the observed data for the HB inversion. In contrast, the LS inversion exhibited slight deviations from the observed data at frequencies ranging from 1 Hz to 0.5 Hz. The weight value (W_1) for most HB inversions was one, except in the low-frequency range (1 Hz–0.0178 Hz). Similarly, the calculated inversion data for d_b also demonstrated a good fit with the observed data for the HB inversion. In contrast, slight deviations from the observed data

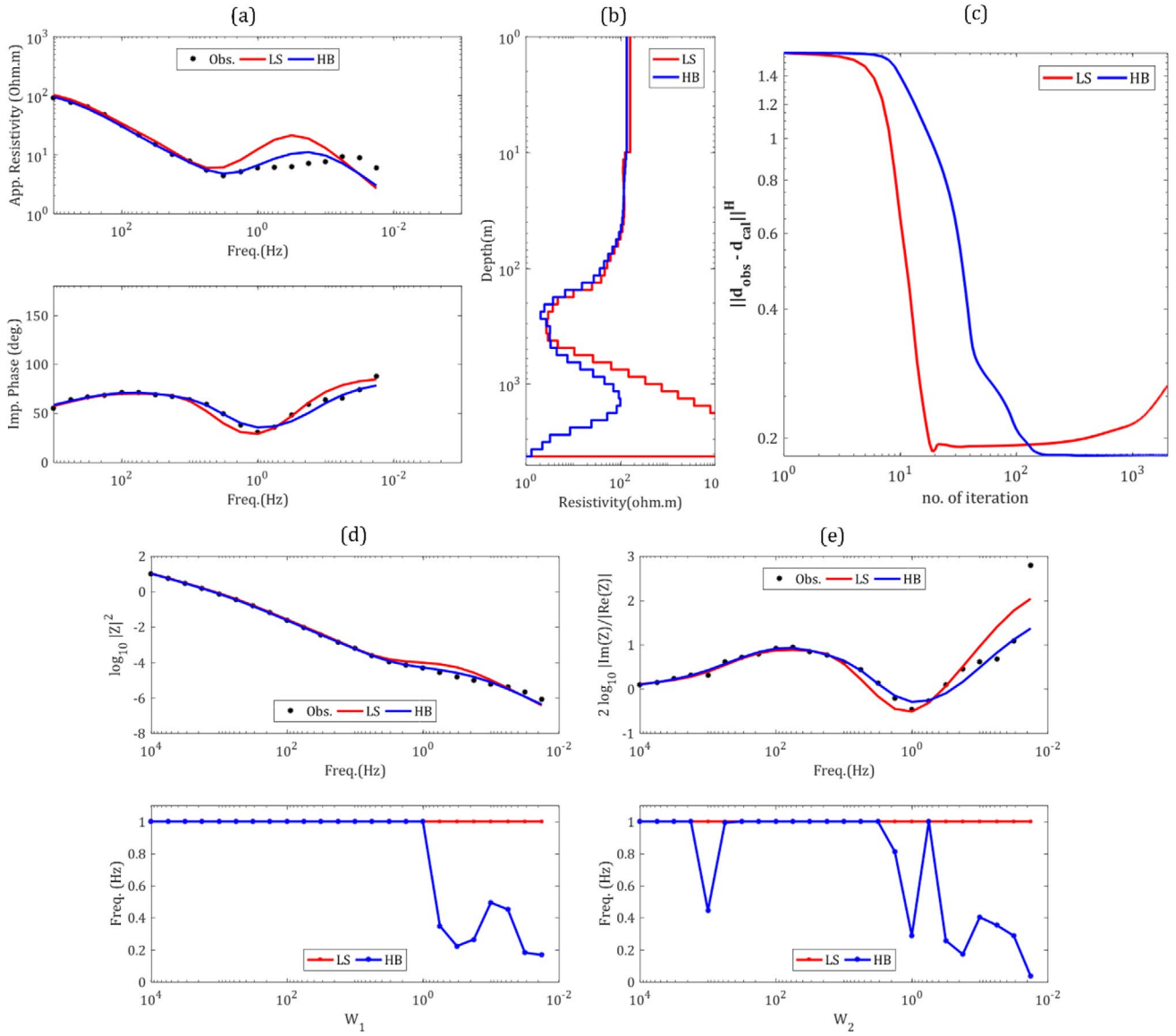

Fig. 9 Huber loss (HB) vs. least-squares (LS) inversion model results for Muara Laboh MTML-xy area **a** Inversion results of the model response, **b** The inversion result model, **c** Misfit, **d** Results of the inversion of data 1 and weights, **e** Results of the inversion of data 2 and weights

Table 3 Misfit comparison of the HB and LS inversions for various cases

Model	HB		LS	
	converge at iteration-	Misfit	converge at iteration-	Misfit
Model 1	168th	0. 000099	180th	0.000099
Model 2	141th	0.000205	154th	0.000205
Model 1 with outlier	25th	0.1937	20th	0.2350
MTP-xy in Patuha area Located in Java Lat: -7.174028 Long: 107.388083	37th	0.06953	20th	0.07038
MTM-yx in Matindok area Located in Sulawesi Lat: -1.393444 Long: 122.306972	60th	0.3069	75th	0. 3326
MTML-xy in Muara Laboh area Located in Sumatra Lat: -1.637693 Long: 101.134747	152th	0. 1848	44th	0.3137
MTU-xy in Ulumbu area Located in East Nusa Tenggara Lat: -8.711222 Long: 120.441278	46th	2.6747	14th	2. 8998

were seen at frequencies ranging from 50 Hz to 0.0178 Hz for the LS inversion. The weight value (W_2) for most HB inversions was one, except at a frequency of 1000 Hz and in the low-frequency range (0.5 Hz–0.0178 Hz).

The results of the xy data inversion for the Ulumbu area can be seen in Fig. 10. The inversion results for the data MTU-xy of the Ulumbu area are also displayed in Fig. 10. The MTU-xy point data for the Ulumbu area (frequency range 320 Hz–0.00034 Hz) were of poor quality, with many outliers, as per the previously established criteria. The data contained several outliers occurring at a frequency of around 100 Hz and at a frequency of 1 Hz at lower frequencies. Furthermore, the data were not smooth and had significant errors or deviations, and the values obtained were not relevant to geothermal field measurements where two conductive zones were present between the resistive zones. A significant difference was observed between the HB and LS inversion results (Fig. 10a). While the HB inversion results aligned well with the observation data, the LS inversion results deviated significantly. The HB inversion model revealed a conductive anomaly at a depth of 100 m to 1000 m. In contrast, the LS inversion showed a random pattern, making analysis difficult (Fig. 10b). The HB inversion reached convergence at the 46th iteration out of 3000 iterations, with a misfit of 2.6747 (Fig. 10c). On the other hand, the LS inversion converged on the 14th iteration, also out of 3000 iterations, with a misfit of 2.8998 (Fig. 10c). The comparison between observation data and calculated data, as well as the weight values of each data d_a and d_b, are presented in Fig. 10d and e. The calculated inversion data for $d_a$exhibited a good fit with the observational data in the HB inversion, while the LS inversion slightly deviated from the observed data at frequencies between 76 Hz and 0.00034 Hz. The weight value W_1 for the HB inversion varied because of the presence of outliers. In the HB framework, small weights were assigned to data points considered outliers, and vice versa, as shown in Fig. 10d and e. The calculation data of the inversion results for $d_b$in the HB inversion showed a fitting pattern with the observation data. In contrast, there was a slight increase in frequencies below 10^{-2} Hz in the LS inversion results. Similar to W_1, the weight value on W_2 for the HB inversion also varied depending on the outlier values in the data.

Based on these results, it can be stated that for data of good quality, both the HB and LS inversion schemes will produce equally good models (Table 3). However, for data of poor quality, the HB inversion is significantly better at handling outliers than the LS inversion scheme. This is evident from the resulting misfit values (Table 3). In the case of good-quality data, the HB inversion yielded a misfit nearly identical to that of the LS inversion. Conversely, for poor-quality data, the HB inversion produced a misfit smaller than that of the LS inversion.

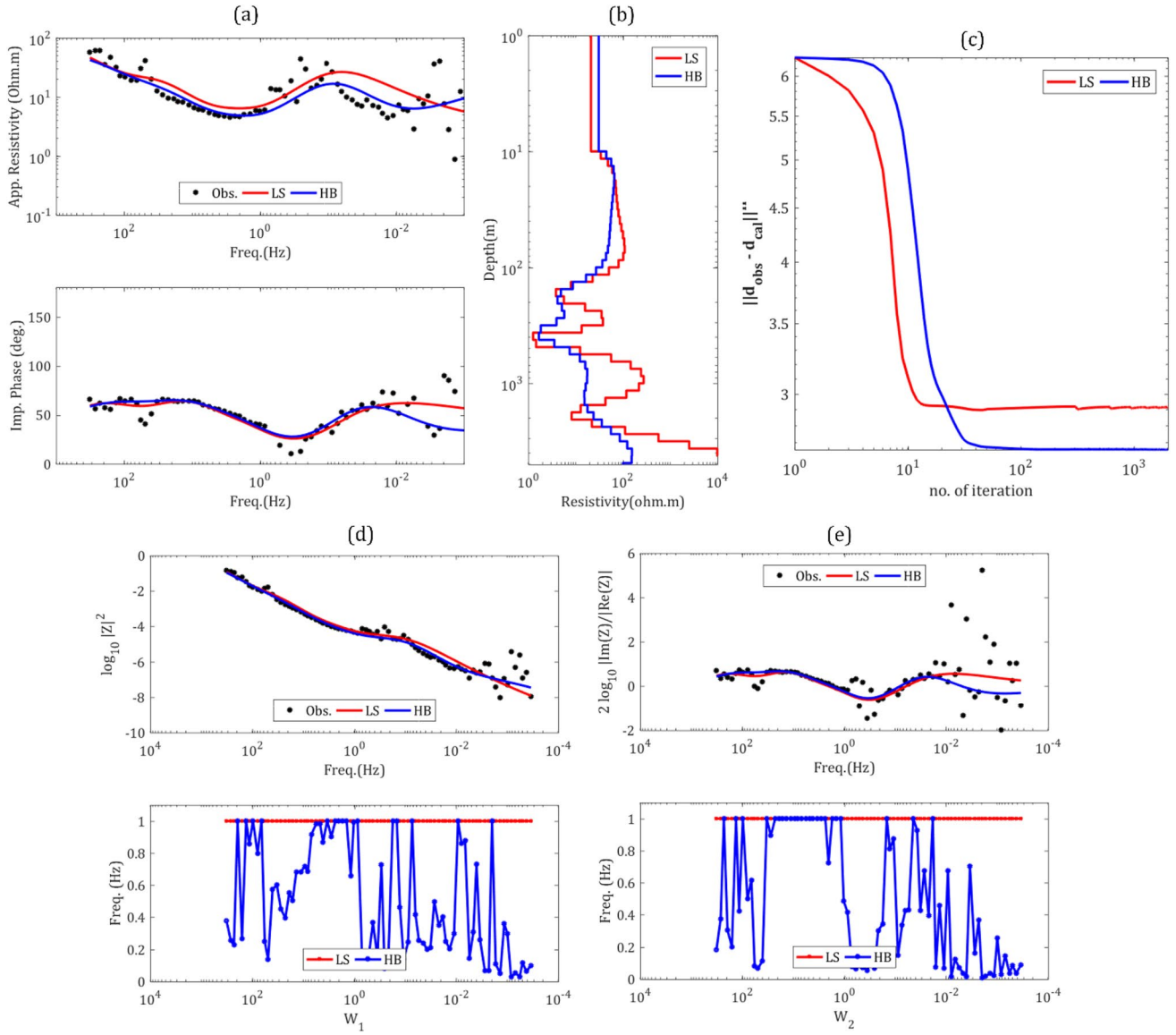

Fig. 10 Huber loss (HB) vs. least-squares (LS) inversion model results for the Ulumbu MTU-xy area **a** Inversion results of the model response, **b** The inversion result model, **c** Misfit, **d** Results of the inversion of data 1 and weights, **e** Results of the inversion of data 2 and weights

4 Conclusion

In this study, successful MT 1D modeling was conducted for both forward and inversion modeling. The forward modeling scheme uses a recursive formulation to generate 1D MT responses for various models, which has been verified to be accurate. The inversion results for synthetic data without outliers demonstrated similar outcomes for both inversion schemes (HB and LS inversions). However, when synthetic data with outliers was considered, a notable difference was observed between the results obtained from HB and LS inversions. The inversion results for some field data exhibited similar outcomes. For field data of good quality, both HB and LS inversions produced equally accurate models. However, for field data of poor quality, the inversion results diverged. For this field data, the HB inversion converged at the 46th iteration out of 3000 iterations, with a misfit of 2.6747, while the LS inversion converged at the 14th iteration out of 3000 iterations, with a misfit of 2.8998. The calculated inversion data showed a good fit with the observed data in the case of HB inversion. Meanwhile, the LS inversion deviated slightly from the observed data in the frequency range for 76 Hz to 0.00034 Hz. Regarding the calculation data of the inversion results for d_b, the HB inversion still matched the observed data pattern. In contrast, the LS inversion results slightly increased at frequencies below 10^{-2} Hz. For field data of poor quality, specifically those containing outliers,

the HB inversion scheme outperformed the LS inversion scheme in handling the data. Based on these results, it can be concluded that the robust inversion with HB outperforms the LS inversion scheme in handling data with outliers, demonstrating its effectiveness for modeling such data.

Acknowledgements This work was supported by Indonesian Education Scholarships (BPI) provided by the Center for Higher Education Fund (BPPT) or Center or Education Services (Pusat Layanan Pendidikan) Ministry of Education, Culture, Research, and Technology of the Republic of Indonesia and the Indonesia Endowment Fund for Education (LPDP) under contract 1646/J5/KM.01.00/2021.

Data availability The datasets generated for this study are available on request to the corresponding author.

Declarations

Conflict of interest The authors declare that they have no conflicts of interest.

References

1. Cagniard, L.: Basic theory of the magneto-telluric method of geophysical prospecting. Geophysics. **18**(3), 497–724 (1953). https://doi.org/10.1190/1.1437915
2. Wait, J.R.: Theory of magnetotelluric fields. J. Res. Natl. Inst. Stand. Technol. Sect. D: Radio Propag. **66D**(5), 509–541 (1962). https://doi.org/10.6028/jres.066d.052
3. Jones, A.G.: Electrical conductivity of the continental lower crust. In: Fountain, D.M., Arculus, R.J., Kay, R.W. (eds.). Continental Lower Crust. Amsterdam, Elsevier, 81–143 (1992)
4. Mackie, R.L., Madden, T.R.: Three-dimensional magnetotelluric inversion using conjugate gradient. Geophys. J. Int. **115**(1), 215–229 (1993). https://doi.org/10.1111/j.1365-246X.1993.tb05600.x
5. Ishizu, K., Ogawa, Y., Mogi, T., Yamaya, Y., Uchida, T.: Ability of the magnetotelluric method to image a deep conductor: exploration of a supercritical geothermal system. Geothermics **96**, 102205 (2021). https://doi.org/10.1016/j.geothermics.2021.102205
6. Fuentes-Arreazola, M.A., Núñez, D., Núñez-Cornú, F.J., Calderón-Moctezuma, A., Ruiz-Aguilar, D., Romo-Jones, J.M.: Magnetotelluric imaging of the Ceboruco Volcano, Nayarit, Mexico. J. Volcanol. Geotherm. Res. **418**, (2021). https://doi.org/10.1016/j.jvolgeores.2021.107339
7. Amatyakul, P., Wood, S.H., Rung-arunwan, T., Vachiratienchai, C., Prommakorn, N., Chanapiwat, P., Siripunvaraporn, W.: An assessment of a shallow geothermal reservoir of Mae Chan hot spring, northern Thailand via magnetotelluric surveys. Geothermics **95**, 102137 (2021). https://doi.org/10.1016/j.geothermics.2021.102137
8. Alpine, F., Yatini, Y., Takodama, I.: Identification of geothermal system in Diana area, Indonesia based on magnetotelluric data modelling. J. Geosci. Eng. Environ. Tech. **7**(1), 7–14 (2022). https://doi.org/10.25299/jgeet.2022.7.1.7448
9. Orange, A.S.: Magnetotelluric exploration for hydrocarbons. Proc. IEEE **77**(2), 287–317 (1989). https://doi.org/10.1109/5.18627
10. Grandis, H., Widarto, D.S., Hendro, A.: Magnetotelluric (MT) method in hydrocarbon exploration: a new perspective. J. Geof. **2**, 14–19 (2004)
11. Firda, S.I., Permadi, A.N., Supriyanto, Suwardi, B.N.: Hydrocarbon reservoir identification in volcanic zone by using magnetotelluric and geochemistry information hydrocarbon reservoir identification in volcanic zone by using magnetotelluric and geochemistry information. IOP Conf. Ser. : Earth Environ. Sci. **132**, 0–5 (2016). https://doi.org/10.1088/1755-1315/132/1/012018
12. Patro, P.K.: Magnetotelluric studies for hydrocarbon and geothermal resources: examples from the Asian Region. Surv Geophys **38**, 1005–1041 (2017). https://doi.org/10.1007/s10712-017-9439-x
13. Zhang, P., Chouteu, M.: The use of magnetotellurics for mineral exploration: an experiment in the Chibougamau region of Quebec. Can J Earth Sci **29**(4), 621–635 (2011). https://doi.org/10.1139/e92-054
14. Robertson, K., Thiel, S., Robertson, K., Thiel, S.: Detecting the fingers of god : optimising magnetotelluric survey design for mineral exploration. ASEG Ext. Abstr. **2019**(1), 1–3 (2019). https://doi.org/10.1080/22020586.2019.12073002
15. Jiang, W., Duan, J., Doublier, M., Clark, A., Schofield, A., Brodie, R.C., Goodwin, J.: Application of multiscale magnetotelluric data to mineral exploration: an example from the East Tennant region, Northern Australia. Geophys J Int **229**(3), 1628–1645 (2022). https://doi.org/10.1093/gji/ggac029
16. Jupp, D.L.B., Vozoff, K.: Two-dimensional magnetotelluric inversion. Geophys J R Astron Soc **50**(2), 333–352 (1977). https://doi.org/10.1111/j.1365-246X.1977.tb04177.x
17. Vozoff, K.: The magnetotelluric method. In: Nabighian (ed.) Electromagnetic Methods in Applied Geophysics, vol. 2, pp. 641–711. SEG Publication, Tulsa (1987)
18. Rousseeuw, P.J., Hubert, M.: Robust statistics for outlier detection. Wiley Interdiscip Rev. Data Min. Knowl. Discov **1**(1), 73–79 (2011). https://doi.org/10.1002/widm.2
19. Sutarno, D., Fatrio, I.: Robust M-Estimation of CSAMT impedance functions. Indones J. Phys. **18**(3), 81–85 (2007)
20. Carbonari, R., D'Auria, L., Di Maio, R., Petrillo, Z.: Denoising of magnetotelluric signals by polarization analysis in the discrete wavelet domain. Comput Geosci **100**(1), 135–141 (2017). https://doi.org/10.1016/j.cageo.2016.12.011
21. Jing-Tian, T., Zhi-Min, X., Xiao, X., Jin, L.: Effect rules of strong noise on magnetotelluric (MT) sounding in the Luzong ore cluster area. Chin. J. Geophys. Chin. Ed. **55**(12), 4147–4159 (2012)
22. Garcia, X., Jones, A.G.: Dead band using the continuous wavelet transform. Geophys **73**, F223–F234 (2008)
23. Egbert, G.D., Booker, J.R.: Robust estimation of geomagnetic transfer functions. Geophys J R Astron Soc **87**(1), 173–194 (1986). https://doi.org/10.1111/j.1365-246X.1986.tb04552.x
24. Chave, A.D., Thomson, D.J., Ander, M.E.: On the robust estimation of power spectra, coherences and, transfer functions. J Geophys Res **92**(B1), 633–648 (1987). https://doi.org/10.1029/JB092iB01p00633
25. Smirnov, M.Y.: Magnetotelluric data processing with a robust statistical procedure. Geophys J Int **152**(1), 1–7 (2003)

26. Sims, W.R., Bostick, F.X., Smiths, H.W.: The estimation of magnetotelluric impedance tensor elements from measured data. Geophys **36**, 938–942 (1971)
27. Gamble, T.D., Goubau, W.M., Clarke, J.: Magnetotellurics with a remote magnetic reference. Geophys **44**(1), 53–68 (1979). https://doi.org/10.1190/1.1440923
28. Smirnov, M.Y., Egbert, G.D.: Robust principal component analysis of electromagnetic arrays with missing data. Geophys J Int **190**(3), 1423–1438 (2012). https://doi.org/10.1111/j.1365-246X.2012.05569.x
29. Yan, J., Zhao, X., Guo, X., Hu, T.: Magnetotelluric impedance estimation based on clustering analysis. J Appl Geophys **189**, 104322 (2021). https://doi.org/10.1016/j.jappgeo.2021.104322
30. Junge, A.: Characterization of and correction for cultural noise. Surv Geophys **17**, 361–391 (1996). https://doi.org/10.1007/BF01901639
31. Sutarno, D.: Development of robust magnetotelluric impedance estimation: a review. Indones J. Phys. **16**(3), 79–89 (2005)
32. Siripunvaraporn, W.: Three-dimensional magnetotelluric inversion: an introductory guide for developers and users. Surv Geophys **33**, 5–27 (2012). https://doi.org/10.1007/s10712-011-9122-6
33. Yu, N., Li, R., Kong, W., Gao, L., Wu, X., Wang, E.: A hybrid grid-based finite-element approach for three-dimensional magnetotelluric forward modeling in general anisotropic media. Comput Geosci **159**, 105035 (2022). https://doi.org/10.1016/j.cageo.2022.105035
34. Bai, N., Zhou, J., Hu, X., Han, B.: 3D edge-based and nodal finite element modeling of magnetotelluric in general anisotropic media. Comput Geosci **158**, 104975 (2022). https://doi.org/10.1016/j.cageo.2021.104975
35. Oryński, S., Jóźwiak, W., Nowożyński, K., Klityński, W.: Comparison of 3D, 2D, and 1D magnetotelluric inversion results on the example of data from Fore-Sudetic monocline. Int. J. Geophys. **2022** (2022). https://doi.org/10.1155/2022/3400950
36. Chouteau, M., Zhang, P., Chapellier, D.: Computation of apparent resistivity profiles from VLF-EM data using linear filtering. Geophys Prospect **44**, 215–232 (1996)
37. Zhou, J., Hu, X., Xiao, T.: A regularized magnetotelluric inversion with a minimum support gradient constraint*. Earthq Sci **33**(3), 130–140 (2020). https://doi.org/10.29382/eqs-2020-0130-03
38. Xiang, Y., Yu, P., Zhang, L., Feng, S., Utada, H.: Regularized magnetotelluric inversion based on a minimum support gradient stabilizing functional. Earth Planet Space. **69,** (2017). https://doi.org/10.1186/s40623-017-0743-y
39. Constable, S.C., Parker, R.L., Constable, C.G.: Models from electromagnetic sounding data. Geophys **52**, 289–300 (1987)
40. Tyler H., Spiteri, R., Szmigielski, J.: One-dimensional magnetotelluric inversion with radiation boundary conditions. Can. Appl. Math. Quart. **15**(4), (2007)
41. Seillé, H., Visser, G.: eliable 1D magnetotelluric probabilistic inversion considering modelling assumption violations. Explor. Geophys. **2019**(1), (2019). https://doi.org/10.1080/22020586.2019.12073113
42. Yi, M.-J., Kim, J.H.: Enhancing the resolving power of least-squares inversion with active constraint balancing. Geopyhs **68**(3), 931–941 (2003). https://doi.org/10.1190/1.1581045
43. Matsuno, T., Chave, A.D., Jones, A.G., Muller, M.R., Evans, R.L.: Robust magnetotelluric inversion. Geophys J Int **196**(3), 1365–1374 (2014). https://doi.org/10.1093/gji/ggt484
44. Nabighian, M.N.: Electromagnetic methods in applied geophysics. Society of Exploration, vol. 2, p. 641. SEG Publication, Tulsa (1988)
45. Menke, W.: Geophysical data analysis: discrete inverse theory. Academic Press Inc, San Diego California (1989)
46. Maithya, J., Fujimitsu, Y.: Analysis and interpretation of magnetotelluric data in characterization of geothermal resource in Eburru geothermal field, Kenya. Geothermics **81**, 12–31 (2019). https://doi.org/10.1016/j.geothermics.2019.04.003
47. Zhang, L., Hao, T., Xiao, Q., Wang, J., Zhou, L., Qi, M., Cui, X., Cai, N.: Magnetotelluric investigation of the geothermal anomaly in Hailin, Mudanjiang, northeastern China. J Appl Geophys **118**, 47–65 (2015). https://doi.org/10.1016/j.jappgeo.2015.04.006
48. Srigutomo, W., Kagiyama, T., Kanda, W., Munekane, H., Hashimoto, T., Tanaka, Y., Utada, H., Utsugi, M.: Resistivity structure of Unzen Volcano derived from time domain electromagnetic (TDEM) survey. J Volcanol Geotherm Res **175**, 231–240 (2008). https://doi.org/10.1016/j.jvolgeores.2008.03.033
49. Malleswari, D., Veeraswamy, K., Azeez, A., Gupta, K.K., Babu, A.K., Patro, N., Harinarayana, P.K.: Magnetotelluric investigation of lithospheric electrical structure beneath the Dharwar Craton in south India: evidence for mantle suture and plume-continental interaction. Geosci Front **10**, 1915–1930 (2019). https://doi.org/10.1016/j.gsf.2018.10.011
50. Telford, W.M., Geldart, L.P., Sheriff, R.E.: Applied geophysics. Cambridge University Press, New York (1990)